

Article

Gas Content Evaluation of Coalbed Methane Reservoir in the Fukang Area of Southern Junggar Basin, Northwest China by Multiple Geophysical Logging Methods

Xu Ge ^{1,2}, Dameng Liu ^{1,2}, Yidong Cai ^{1,2,*} and Yingjin Wang ^{1,2}

¹ School of Energy Resources, China University of Geosciences, Beijing 100083, China; 3006150035@cugb.edu.cn (X.G.); dmliu@cugb.edu.cn (D.L.); 3006160030@cugb.edu.cn (Y.W.)

² Coal Reservoir Laboratory of National Engineering Research Center of CBM Development & Utilization, China University of Geosciences, Beijing 100083, China

* Correspondence: yidong.cai@cugb.edu.cn; Tel.: +86-10-8232-2754

Received: 11 June 2018; Accepted: 11 July 2018; Published: 17 July 2018



Abstract: To study the gas potential of coalbed methane (CBM) in the Fukang area, southern Junggar Basin (SJB) of North China, different methods including multiple geophysical logging, the Kim method with proximate analysis data, and Langmuir adsorption were used to evaluate the gas content. Furthermore, the geological controls on gas content were evaluated. One hundred sixteen CBM wells with geophysical logging and 20 with field-measured gas content were adopted to assess the gas content in the Fukang area of SJB, NW China. The results show that the two geophysical logging variables (DEN and CNL) were favorable for evaluating the gas content due to the perfect correlation with the measured gas content. The gas content varies from 4.22 m³/t to 16.26 m³/t, and generally increases with increasing burial depth. The gas content in coal seams along the synclinal axis is significantly higher than that along the synclinal wing in the west zone. In the east zone, the gas content of the westward is higher than that of the eastward because of the fault coating effect by reverse fault. Generally, the gas content of the SJB is in the order of syncline > surrounding reverse fault > slope of syncline > slope of anticline > central of reverse fault, if only geological structure features are considered. The favorable areas for CBM concentration appear to be a composite gas controlling result of multiple geological factors. Two typical geological scenarios with low gas content and high gas content were revealed. In the Fukang area of SJB, the low gas content is mainly due to the normal fault and roof lithology of sandstone. The most favorable area of high gas content for CBM exploration and development is in the northeast, where reversed fault, synclinal axis, mudstone roof lithology, and burial depth coincide with high gas content.

Keywords: coalbed methane; gas content; geophysical logging; controlling factors; southern Junggar Basin

1. Introduction

Coalbed methane is a type of unconventional gas resource [1], the exploration and exploitation of which have been intensively implemented [2–7]. Gas content is critical for CBM exploration and can be affected by multiple factors including structural type, lithology, thickness, coal rank, and burial depth [8]. Previous research revealed that structurally controlled gas content has the pattern of syncline > slope of syncline > slope of anticline > anticline > central of normal fault > surrounding normal fault [7]. Lithology-controlled gas content shows that the mudstones generally preserve the high gas content [9]. A moderate burial depth (~500–800 m), a relatively high coal rank (~1.25–1.55%), and a favorable coal thickness no less than 5 m could also effectively promote gas enrichment [10,11].

The gas content in the syncline is obviously preferable, and the reverse faulting is more advantageous to gas enrichment than the normal faulting in the middle SJB [12].

Gas contents can generally be evaluated through field measurements, geophysical logging analysis, and proximate analysis [13–23]. By assuming a standard moisture and ash content, and using the hydrostatic head to estimate pressure, the relationship of rank and depth versus gas content can be constructed. The Kim method combined with logging data was first used to evaluate the gas content of coal seams in the San Juan basin [13]. Subsequently, the ash yields and Langmuir isotherms were adopted to assess the gas content in the northern San Juan basin [14]. Geophysical logging uses electrical, magnetic, nuclear, and acoustic methods to measure the petrophysical properties of formations and fluids around the boreholes [15–20], as listed in Table 1. The conventional logs including resistivity, DEN, AC, GR, and photoelectric absorption were employed to enhance the accuracy of the gas content evaluation in coalfields, namely Jharia (bituminous) and Barmer sanchole (lignite) of India [21]. The multiple regressions include RLLD, AC, CNL, DEN, GR, and the buried depth of coal seams were used to construct a logging prediction model of the gas content [22]. The gas content predicted through the Langmuir equation was used to analyze the factors influencing the gas production in the southern Qinshui Basin, North China [23].

The research area can be divided into two parts: 52 CBM wells in the west area and 64 wells in the east area. Serial coal seams developed in the study area include the Nos. 39, 41, 42, 43, 45-1, and 45-2 coal seams, and the burial depth of coal seams are from 517 m to 1450 m. In this work, the logging data of RLLS, RLLD, GR, CNL, and DEN combined with experimental data (moistures, ash yields, volatiles and fixed carbon) of 116 boreholes from the Fukang area in the SJB are used to evaluate the gas content of the serial coal seams of the lower Jurassic Formation. Multiple methods are used to predict the gas content, and the best one was chosen to make a prediction in the Fukang area of the SJB in the absence of measured data. Next, the horizontal and vertical gas content variation is evaluated and discussed. Finally, the geological controlling factors of CBM enrichment in the SJB are discussed. Both the gas content prediction and the controlling factors analysis was performed for the first time in the Fukang area of SJB.

Table 1. Comprehensive table of the gas content models.

Method	Name	Suitable Conditions	Specific Model
Statistical analysis method	Wang Z.W., 2010		$V_g = -a\rho + b$
			$V_g = aA_{ad}^b$
	Pan H.P., 1998		$V_g = a + bh + c(1 - A) + dQ_c$
Langmuir equation method	Fu X.H., 2009		$V_g = a\rho + bG + cC_{NL} + dA + e$
			$V_g = V_L P / (P + P_L)$
	Hawkins J.M., 1992		$V_g = (1 - A - w) \frac{V_L P}{P + P_L} S_g$
Conventional ash content measurement method		If lack of Langmuir experiment data	$\lg V_L = a \lg(V_{F_c} / V_{V_m}) + b$ $\lg P_L = c \lg(V_{F_c} / V_{V_m}) + d$
		The maximum pressure is 930 psi	$V_g = (1 - w - A)[k_0 P^{n_0} - BT] \frac{V_w}{V_d}$
	Kim A.G., 1977	If P is assumed to equal the hydrostatic head	$V_g = (1 - w - A)[k_0(0.096h)^{n_0} - B(\frac{1.8h}{100} + 11)] \frac{V_w}{V_d}$
		Assuming the pressure is homogeneous	$V_g = C_p(1 - w - A)$
	Mavor M.J., 1995		$V_g = 18.77 - 23.47 \frac{A}{1-w}$
	Mullen M.J., 1990		$V_g = 32.87 - 16.92\rho_b$

V_g : gas content (cm^3/g); Q_c : fixed carbon mass fraction (%); ρ : density (g/cm^3); G : natural gamma ray (API); R : resistivity ($\Omega\text{-m}$); Δt : sonic transit-time (us/ft); C_{NL} : neutron porosity (%); a , b , c , d , e : undetermined coefficients; P : pressure of coal reservoir (MPa); V_L : Langmuir volume (cm^3/g); P_L : Langmuir pressure (MPa); S_g : adsorbed gas saturation (%); w : water mass fraction (%); A : ash mass fraction (%); V_w : gas content of wet coal (cm^3/g); V_d : gas content of dry coal (cm^3/g); B : constant is approximately equal to $0.14 \text{ cm}^3/(\text{g}\cdot^\circ\text{C})$; k_0 , n_0 : correction factor, get by fitting coal core sample data; T : coal reservoir temperature ($^\circ\text{C}$); h : the depth; C_p : gas content of pure coal reservoir; ρ_b : bulk density; V_{F_c} : the ratio of fixed carbon; V_{V_m} : volatile matter.

2. Geological Settings

The Junggar Basin is one of the basins that have gas resources over $20 \times 10^{12} \text{ m}^3$ in Xinjiang Uygur Autonomous Region, NW China [4,24]. The predicted CBM resource in Xinjiang Uygur Autonomous Region is $\sim 9.5 \times 10^{12} \text{ m}^3$. The Junggar Basin accounts for about half of the total CBM resources in the Xinjiang Uygur Autonomous Region due to the thick coal seams (20–80 m) [25]. The SJB has abundant low–medium rank coals; the coal rank across the SJB ranges from subbituminous to high-volatile bituminous. The SJB contains CBM concentration of $4.5 \times 10^8 \text{ m}^3/\text{km}^2$ with a maximum gas content of $16.26 \text{ m}^3/\text{t}$. Hence, it becomes another crucial CBM-bearing basin in China [24]. The Fukang area in the SJB develops abundant low-rank coals with $R_{o,m}$ of 0.5–0.8%, and the gas content stabilizes at $\sim 4\text{--}16.26 \text{ m}^3/\text{t}$. The highest CBM production is $17,000 \text{ m}^3$ per day, and the total gas production is $20 \times 10^4 \text{ m}^3$ per day. The Baiyanghe and Sangonghe mining areas are the first CBM pilot projects in the Fukang area of the SJB. The structure, sedimentation and hydrogeology are considered to play “the most important,” “the most basic,” and “a supporting” role, respectively, in the process of CBM accumulation of the Xishanyao Formation in the middle of the southern Junggar Basin. This region is to the west of the study area [26]. With low exploration degree, gas content in the Fukang area still needs to be carefully evaluated, and the geological factors controlling gas content in different coal seams also need to be determined.

2.1. Structural Settings

The SJB, surrounded by a nappe belt of the northern Tianshan Mountains and the Boluokenu-aqikuduk Fault, has an area of $1.8 \times 10^3 \text{ km}^2$ (30 km in width and 60 km in length) (Figure 1a). Tectonically, the geological structures of SJB are mainly a series of NWW thrust faults, EW folds in the west and gentle strata in the east [27]. The SJB formed from Late Hercynian orogeny, and a sedimentary basement was formed in the Early Permian and constructed gradually during Triassic [28]. The SJB has been influenced by the North Tianshan Uplift and the Bogda Mountains since the middle Miocene [29]. Finally, the thrust folds formed in the Cenozoic strata, which were maintained [30].

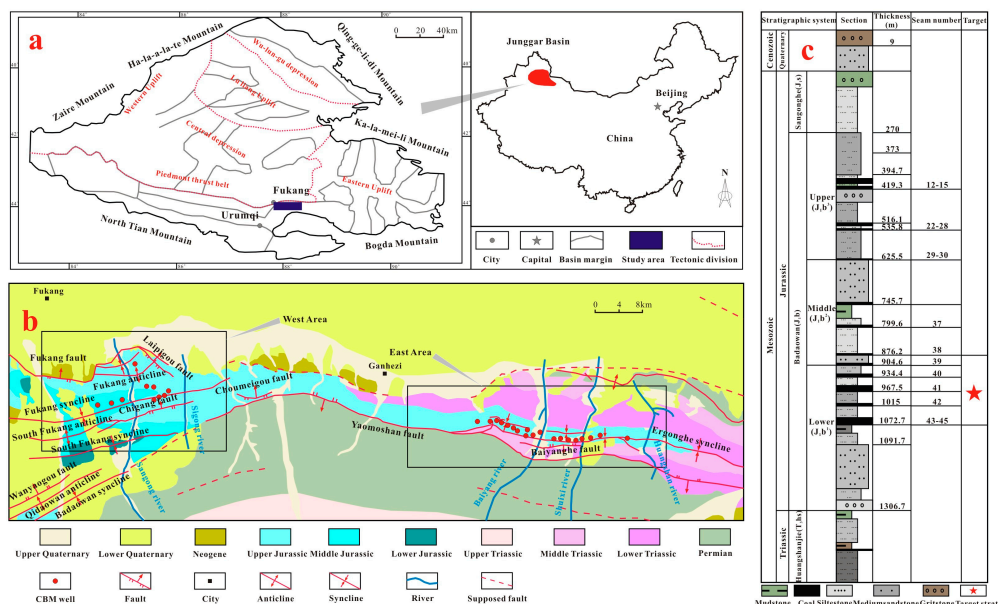


Figure 1. (a) Location and geological structure of study area in the SJB; (b) the distribution map of structural traps and fault systems of the SJB refer to Figure 1a for the study area locations; (c) a map showing stratigraphic section of the SJB, the combinations of the target strata in the Badaowan Formation strata are presented.

2.2. Stratigraphic Characteristics

The formation in the SJB contains the Permian, Triassic, Jurassic, and Quaternary strata. The ground surface of the SJB is mostly covered by the Quaternary strata, and the Jurassic formations are exposed locally [31]. The Badaowan and the Xishanyao Formations are the main coal-bearing strata, and the Sangonghe Formation is located between them with little thin coal seams. As shown in Figure 1c, coal seams are widely spread in the Badaowan formation deposits of the Lower Jurassic (J1b) [26]. Coal seams are up to a few meters thick, and parts of them are interbedded with sandstone and mudstone. The Badaowan Formation mainly developed in fluvial facies and swamp facies, while the Xishanyao Formation developed in delta facies, lacustrine facies, and swamp facies [32]. Total thickness of coal seams was remarkable, and Nos. 39, 41, 42, 43, and 45 were target seams for CBM exploration.

3. Methodology

The gas content measurement is based on the National Standard of China (GBT 28753-2012 and GB/T 19559-2008) [33–35]. The measured gas content includes desorbed gas, lost gas and residual gas [35]. The formula is as follows:

$$V_g = \frac{V_L + V_D}{m_T} + \frac{V_R}{m_R}, \quad (1)$$

where V_g is the gas content (cm^3/g); V_L is the lost gas volume (cm^3); V_D is the desorbed gas volume (cm^3); V_R is the residual gas volume (cm^3); m_T is total sample quality (g); m_R is residual gas quality (g). The measured gas content of the main coal seams ranges from $6.00 \text{ m}^3/\text{t}$ to $16.26 \text{ m}^3/\text{t}$.

3.1. Kim Method with Proximate Analysis Data

The relationship between adsorbed gas volume, pressure and temperature can be described by [13]:

$$V = k_0 P^{n_0} - BT, \quad (2)$$

where V is the volume of gas adsorbed (cm^3/g); P is the pressure of coal reservoir (MPa); B is a constant with an average value of $0.14 \text{ cm}^3/\text{g } ^\circ\text{C}$; k_0 and n_0 are the constants; T is the coal reservoir temperature ($^\circ\text{C}$). The values of k_0 and n_0 can be expressed by the ratio of fixed carbon (V_{F_c}) to volatile matter (V_{V_m}):

$$k_0 = \frac{0.8V_{F_c}}{V_{V_m}} + 5.6, \quad (3)$$

$$n_0 = 0.315 - 0.01 \frac{V_{F_c}}{V_{V_m}}. \quad (4)$$

At a given depth, the pressure P is usually assumed to be equal to the hydrostatic head:

$$P = 0.096h. \quad (5)$$

A commonly used geothermal gradient is $1.8 \text{ }^\circ\text{C}/100 \text{ m}$, and the ground temperature is $11 \text{ }^\circ\text{C}$. The temperature at burial depth of coal seam can be estimated as follows:

$$T = 1.8 \frac{h}{100} + 11. \quad (6)$$

To estimate the gas content, moisture content must be considered in a real coal seam. The calculated gas content is multiplied by the factor:

$$V_g = (1 - w - A) [k_0 P^{n_0} - B(\frac{1.8h}{100} + 11)] \frac{V_w}{V_d}. \quad (7)$$

If P is estimated from the hydrostatic head, the above equation can be substituted:

$$V_g = (1 - w - A)[k_0(0.096h)^{n_0} - B\left(\frac{1.8h}{100} + 11\right)] \frac{V_w}{V_d}, \tag{8}$$

where the value of $\frac{V_w}{V_d}$ can be evaluated through the Kim method [13]. In his study, the $\frac{V_w}{V_d}$ values were distributed between 0.18 and 0.93, and the value decreases with the decrease of coal rank. According to R_o, m (0.5–0.8%) in our research area, the final value of $\frac{V_w}{V_d}$ is 0.55. A comparison between the calculated gas content by Kim method and the measured gas content is shown in Figure 2. All the predicted data have intensive error, especially in the C161 and C131 wells.

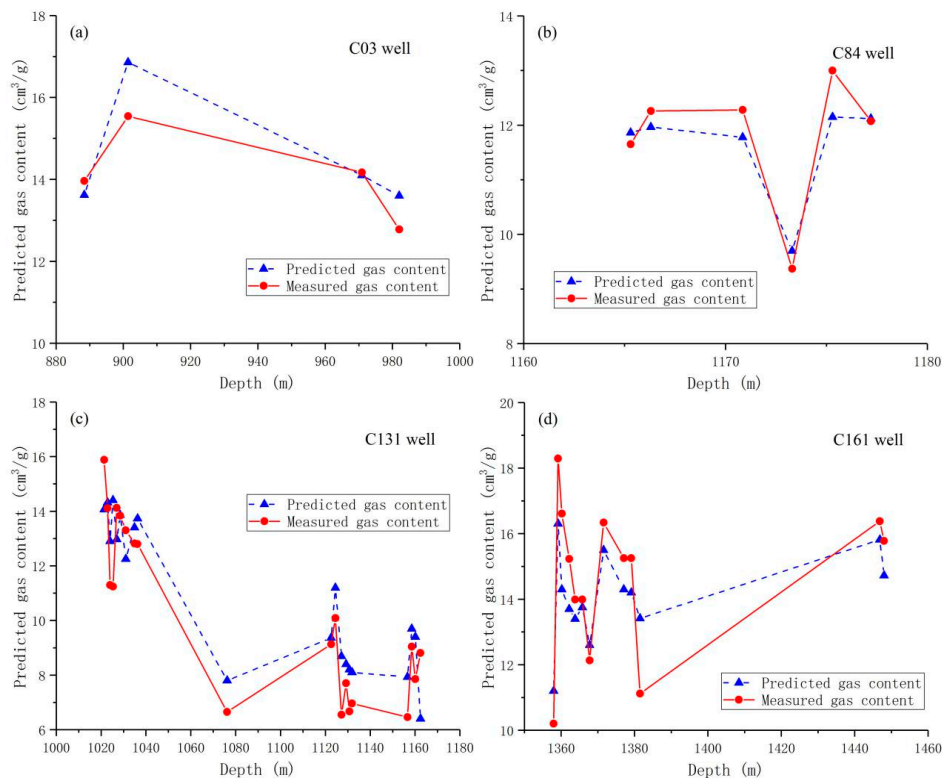


Figure 2. Comparison between predicted and measured gas contents with Kim method in the C03 well (a), C84 well (b), C131 well (c), and C161 well (d).

3.2. Langmuir Method

The gas adsorbed volume can be evaluated through Langmuir theory with isothermal adsorption:

$$V_g = (1 - A) \frac{V_L P}{P + P_L}, \tag{9}$$

where V_g is the gas adsorbed volume (cm³/g); P is the pressure (MPa); P_L is the Langmuir pressure (MPa); A is the dry ash content, weight fraction (%); and V_L is the Langmuir volume (cm³/g).

Gas content can be evaluated by the coefficients of isothermal adsorption, the proximate analysis data, the gas saturation and the reservoir pressure:

$$V_g = (1 - w - A) \frac{V_L P}{P + P_L} S_{gas}, \tag{10}$$

where S_{gas} is the gas saturation (%). The reservoir pressure conforms to the following linear formula if the depth is less than 1600m in the SJB: $P = 0.076h + 3.42$. S_{gas} can be calculated by the measured gas

content. The predicted gas content by Langmuir method is shown in Table 2. The error reaches 30% in some wells (e.g., No. 43 coal seam in the C131 well).

Table 2. The comparative results and error analysis between measured gas content and predicted gas content with Langmuir method.

Well	Seam Number	Depth (m)	S _{gas} (%)	Measured Q _M (cm ³ /g)	Predicted Q _P (cm ³ /g)	$\frac{ Q_P - Q_M }{Q_M} \times 100$ (%)
C84	43	1165.6	71.5	11.65	11.03	5.32
		1173.6		9.37	11.05	17.93
C131	42	989	45.1	8.63	7.16	17.03
		1024.3		11.3	14.7	30.09
	43	1036.5	66.6	12.8	12.09	5.55
		1076.5		9.65	7.56	21.86
	45-2	1122.9	47.1	9.13	9.01	1.31
C161	43	1360.6	63.3	15.61	13.5	13.52
		1377.6		15.25	13.57	11.02
	45-1	1447.1	68.6	15.38	14.4	6.37

3.3. Well Logging Method

Coals can be easily distinguished by geophysical logging [36]. RLLS (shallow laterolog, $\Omega \cdot m$) and RLLD (deep laterolog, $\Omega \cdot m$), reflecting the formation resistivity, can be used to calculate porosity of the formation. AC (acoustic log, us/ft) will increase when the acoustic wave meets the gas layers. Therefore, AC can be used to identify the gas layer and acquire the rock porosity. GR (natural gamma ray log, API), CNL (compensated neutron log, PU), and DEN (density log, g/cm³), belonging to radioactive logs, can be adopted to determine the lithology and estimate the shale content. The above six well logging methods are used in this study, as shown in Figure 3. Although DEN can be used to evaluate the gas content, coal seams with low mechanical strength will lead to borehole expansion. This phenomenon will result in inaccurate DEN values. Therefore, the DEN value needs correction [37]:

$$L_c = L + a(D_{CAL} - D_{bits})/D_{bits} + b, \quad (11)$$

where L is the logging response value before correction; L_c is the corrected logging response value; D_{CAL} is the borehole diameter; D_{bits} is the diameter of drilling bit; a and b are correction coefficients. Log data of 33 samples were used to obtain the value of a and b with Equation (11). In Figure 4, the relationship of the measured gas content and logging curves is plotted. Ash yields can decrease the gas absorption in coal, which positively correlates with the DEN (Figure 4a). Therefore, a negative correlation between gas content and DEN was found as shown in Figure 4b. Generally, a high hydrogen index caused a high CNL response, resulting in a positive relationship (Figure 4c). Gas content has a negative relationship with GR, but was positively correlated with RLLD and AC (Figure 4d–f). Therefore, these well loggings have more or less correlation with the gas content. Here, GR, AC, CNL, DEN, and RLLD were selected to make a comprehensive evaluation of the gas content (V_g):

$$V_g = 42.19 - 17.99DEN - 0.25CNL + 0.02AC - 0.03GR - 5.58e^{-6}LLD \quad (R^2 = 0.88), \quad (12)$$

where the correlations between these five well loggings indicators and the gas content were good. However, this correlation was not adopted to evaluate the gas content due to the absence of the values of RLLD, AC, and GR in the eastern part of the research area. Therefore, DEN and CNL were used to assess the gas content, which shows a good correlation coefficient of 0.89.

$$V_g = 36.25 - 16.32DEN - 0.21CNL \quad (R^2 = 0.89). \quad (13)$$

Table 3 shows the variance analysis. The five and two variables are compared with the measured gas content (Table 4), which shows that two-variable fitting formulas are more accurate than five-variable fitting formulas. The five variables produce much more error compared with the two variables, as shown in Figure 5.

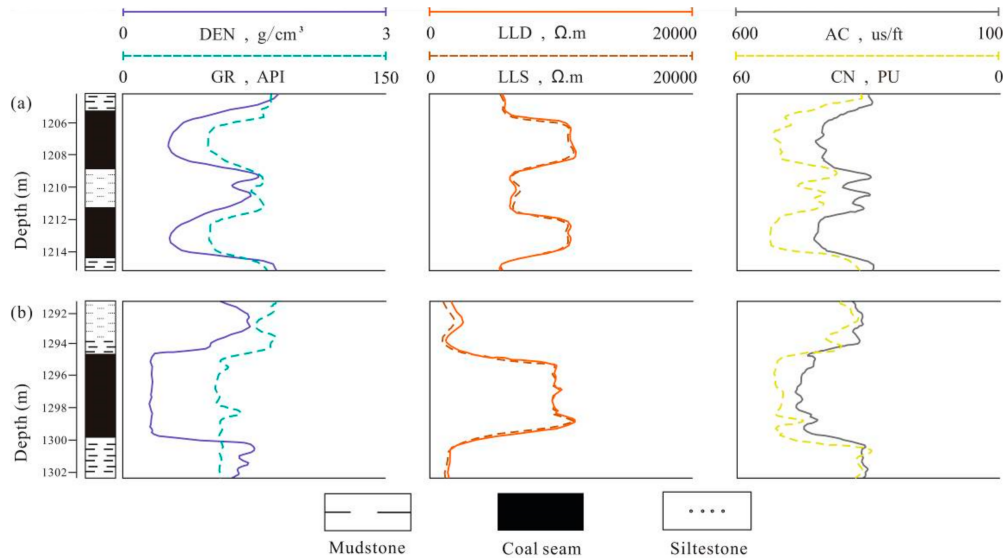


Figure 3. Logging response characteristic of coal reservoirs in the C51 well (a) and C84 well (b).

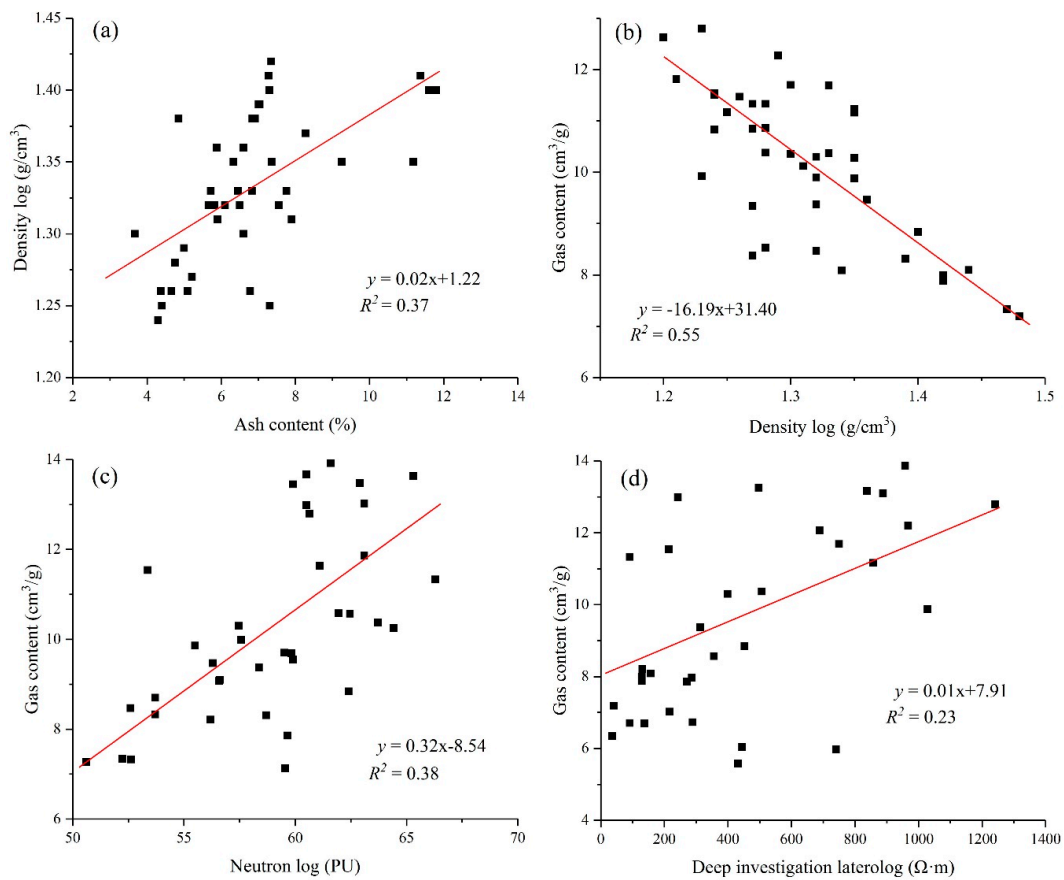


Figure 4. Cont.

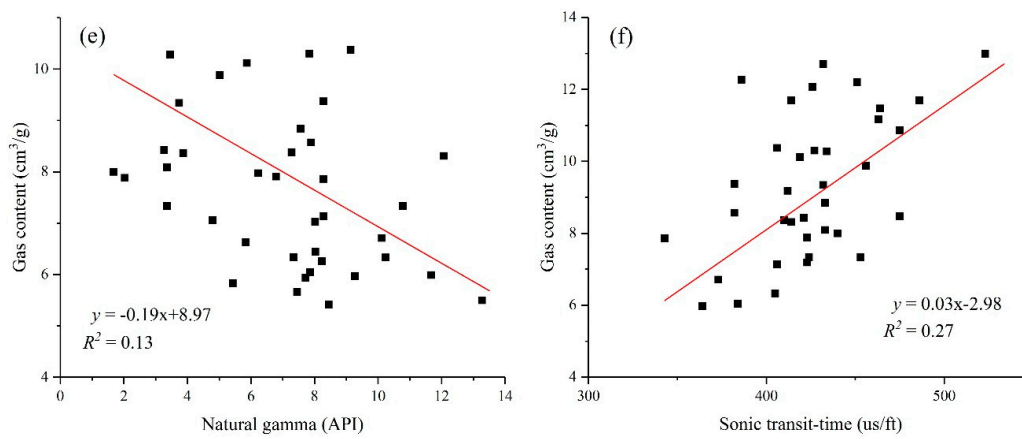


Figure 4. The fitting relationship between density and ash content (a); the fitting relationship between gas content and density (b), neutron (c), deep lateral resistivity (d), natural gamma (e), acoustic time (f).

Table 3. The gas content fitting formulas with CNL and DEN.

Well	Predicted Coalbed Gas Content, cm ³ /g	Samples	Correlation Coefficient	Residual Error	F
C161	$V_g = 36.25 - 16.32DEN - 0.01CNL$	12	0.94	1.50	789.72
C153	$V_g = 55.83 - 22.21DEN - 0.19CNL$	9	0.96	0.18	2163.11
C131	$V_g = 44.97 - 18.19DEN - 0.11CNL$	21	0.91	0.08	3231.81
C84	$V_g = 46.21 - 20.89DEN - 0.06CNL$	6	0.98	0.02	13714.9

Table 4. Measured and predicted gas contents and error analysis.

No.	Well	Measured Q _M (cm ³ /g)	Predicted Q _P 2 Variables	Predicted Q _P 5 Variables	$\frac{ Q_P - Q_M }{Q_M} \times 100$	
					2 Variables	5 Variables
1	C51	6.00	5.13	4.74	14.50	20.99
2	C52	14.89	14.86	15.31	0.18	2.82
3	C53	12.31	10.11	10.82	17.84	12.09
4	C54	4.22	3.30	3.70	21.80	12.23
5	C81	12.77	13.58	13.81	6.33	8.18
6	C82	14.13	14.39	14.74	1.81	4.34
7	C83	14.90	14.71	15.11	1.30	1.41
8	C84	13.45	13.72	14.05	1.99	4.48
9	C06V	13.67	13.89	14.22	1.58	4.04
10	C111	13.02	13.91	14.16	6.81	8.72
11	C112	13.63	14.41	14.65	5.75	7.49
12	C01	14.19	14.21	14.62	0.16	3.02
13	C02	13.29	13.73	14.09	3.29	5.99
14	C03	15.37	14.69	15.24	4.45	0.86
15	C04	14.97	14.70	15.20	1.78	1.56
16	C05	14.66	14.54	15.04	0.79	2.59
17	C1H	15.69	14.17	14.85	9.69	5.34
18	C13X	14.34	14.56	15.02	1.53	4.72
19	C131	13.95	14.23	14.68	1.99	5.26
20	C132	8.04	8.61	8.79	7.04	9.28
21	C133	12.99	13.40	13.79	3.13	6.15
22	C151	14.39	13.86	14.36	3.69	0.18
23	C152	13.95	14.05	14.44	0.68	3.48
24	C153	13.92	14.22	14.57	2.16	4.69
25	C154	13.48	14.07	14.37	4.36	6.63
26	C161	14.03	14.05	14.47	0.13	3.13
27	C162	13.87	14.22	14.66	2.55	5.68
28	C164	14.68	14.71	15.23	0.21	3.75
29	C165	16.26	14.67	15.37	9.76	5.47
30	C166	12.53	12.72	13.18	1.53	5.21

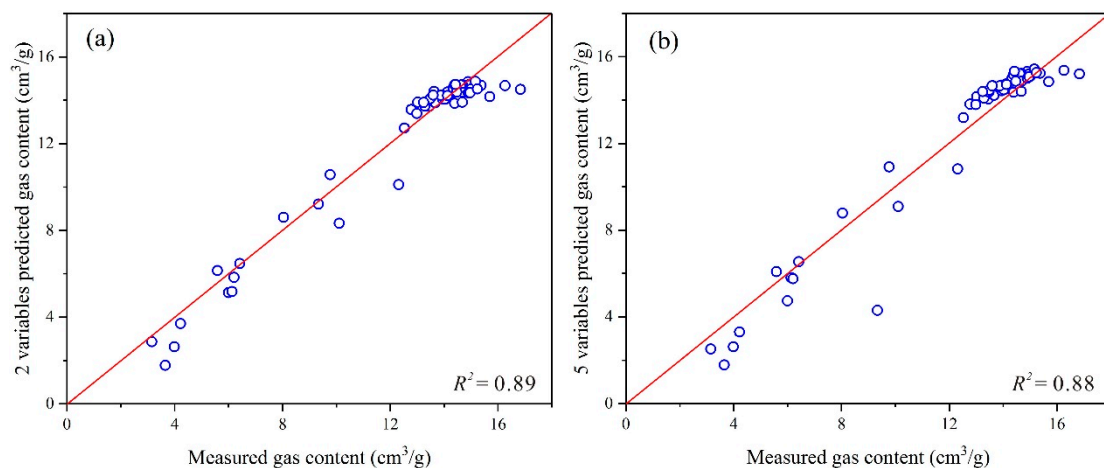


Figure 5. Comparison between measured and two variables' predicted gas contents with logging method (a); comparison between measured and five variables' predicted gas contents with logging method (b).

The logging value of RLLD in coal seam is generally in the range of tens to thousands of $\Omega \cdot \text{m}$. Normally, it is difficult to observe the change of RLLD value when the gas content changes. As a kind of organics rock, coal is a low velocity material for acoustic transmission. Therefore, pores, fractures, liquid, and gas in coals all have a great impact on AC values. GR measures ash in coal seam, which cannot reflect the gas layer directly. Therefore, the AC, GR, and RLLD were reduced in this model to predict the gas content more accurately.

The gas contents produced by the Langmuir method and Kim method are discrete. The logging data was used to fit proximate analysis data through the Kim method, then the value of P_L and V_L was calculated by the proximate analysis data, finally the gas content was obtained [38]. Although the correlation coefficient in previous research [38] can reach 0.73, the correlation coefficients in the study area were too low to predict, with values in the range of 0.06–0.11. Therefore, the two-variable model is selected to predict the gas content as shown in Figure 6, and it can be observed that less error was produced between the predicted and the measured gas contents in this study.

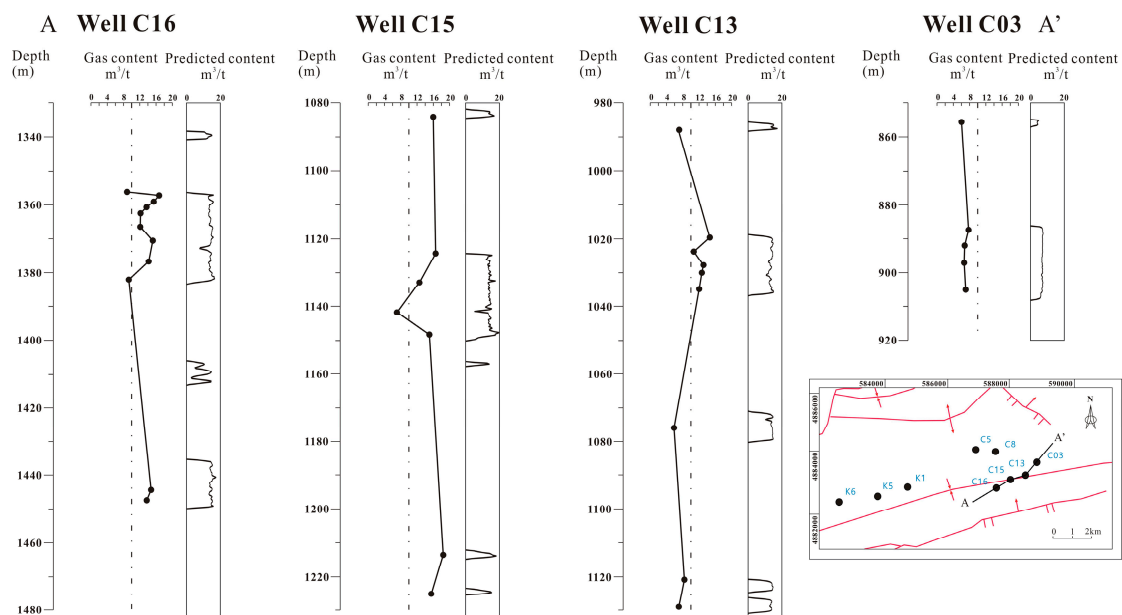


Figure 6. Comparison between predicted and measured gas contents on profile by the logging method with two variables.

4. Results and Discussion

4.1. Gas Content Distribution

The gas content for 33 CBM wells were regionally evaluated by geophysical logging model with two variables as shown in Figures 7–12. The total gas content of the Nos. 39, 41, 42, 43, 45-1 and 45-2 coal seams is in the range of 5.9 to 13.6 m³/t, 6.7 to 13.5 m³/t, 6.3 to 15.9 m³/t, 6.3 to 14.9 m³/t, 5.58 to 14.8 m³/t, and 6.2 to 15.6 m³/t, respectively. As shown in Figure 7a, the gas content is mostly concentrated in the east zone of the No. 39 coal seam, and well K18 in the east zone has high gas content of 13.6 m³/t. The gas content is mostly concentrated in the eastern part of the Ganhezi city of the No. 41 coal seam (Figure 7b). In the Figure 7c, the gas content of the No. 42 coal seam shows an increasing trend from east to west in the study area. In the No. 43 coal seam, the CBM wells K1 and K2 have a low gas content of 7.4 m³/t and 7.1 m³/t; in the western area, other CBM wells generally have a gas content higher than 10 m³/t (Figure 9a); well S58 has high gas content of 14.4 m³/t near the Huangshan River in the east zone (Figure 9b). CBM wells in the No. 45-1 coal seam mostly have gas content more than 10 m³/t, except for wells C13 and C03 (5.6 m³/t and 8.7 m³/t) (Figure 11a). On the contrary, the gas content in the No. 45-2 coal seam for most CBM wells have a gas content lower than 9 m³/t, except CBM wells K5 and C16 (14.1 m³/t and 13.6 m³/t) (Figure 11b). Vertically, the gas content gradually increases with the increasing burial depth of coal seams. In the plane, the high gas content of Nos. 39, 41, 42, and 43 coal seams generally distributes in the western part; the high gas content of Nos. 43, 45-1 and 45-2 coal seams displays in the southern part of the west zone. The gas content distribution was affected by multiple geological factors, as will be elaborated below.

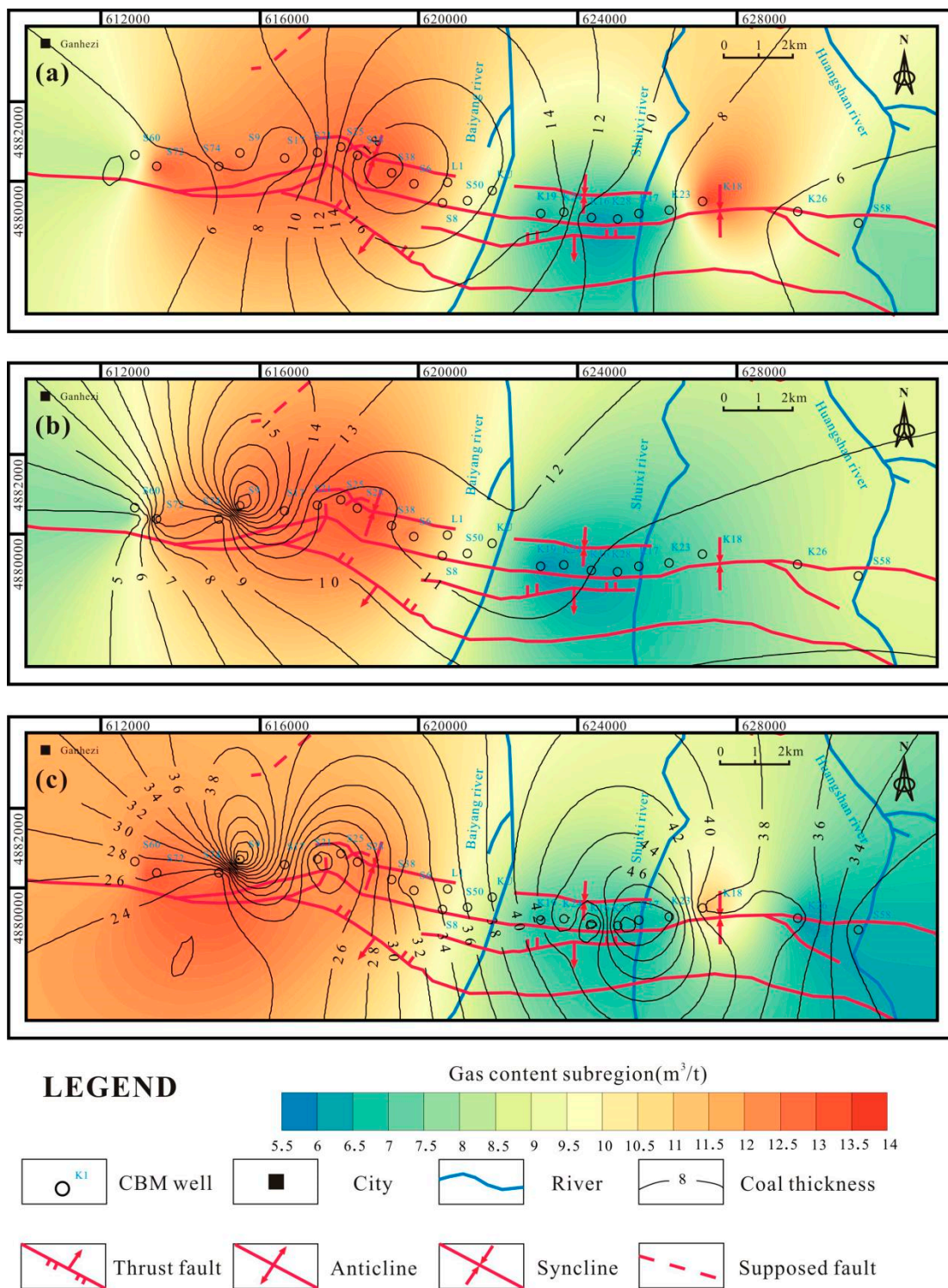


Figure 7. Relationship between gas content and coal thickness of Nos. 39 (a), 41 (b), and 42 (c) coal seams in the Ergonghe syncline (units of contour lines: m for coal thickness and m^3/t for gas content with different color areas).

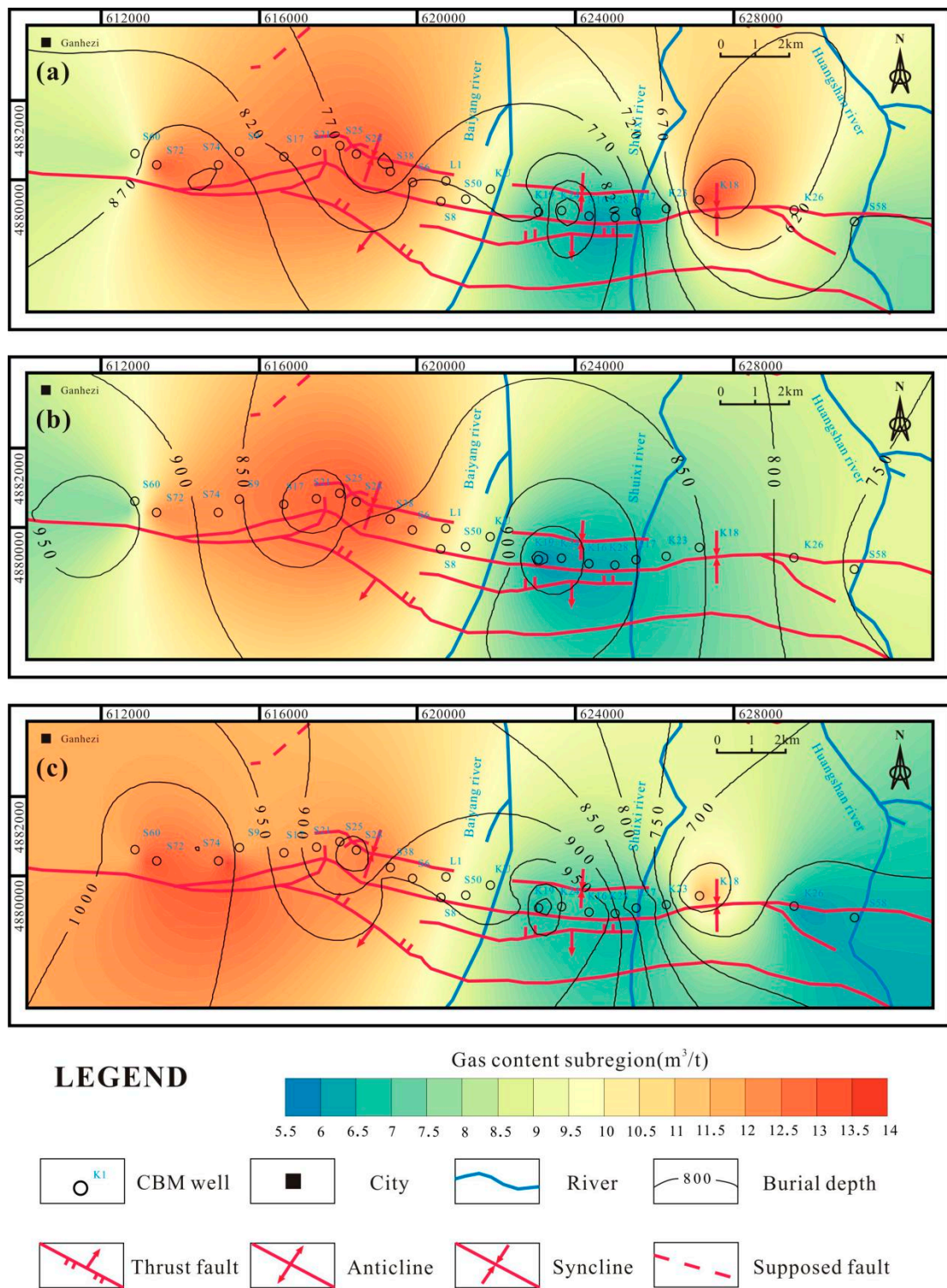


Figure 8. Relationship between gas content and burial depth of Nos. 39 (a), 41 (b), and 42 (c) coal seams in the Ergonghe syncline (units of contour lines: m for burial depth and m^3/t for gas content with different color areas).

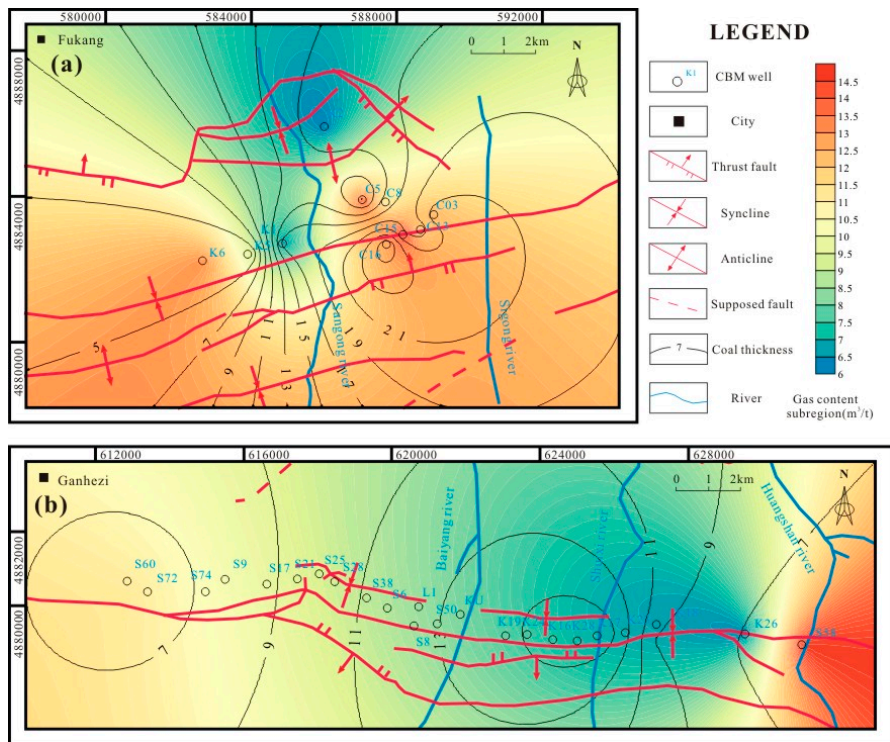


Figure 9. Relationship between gas content and coal thickness of No. 43 coal seam in the Fukang syncline (a) and Ergonghe syncline (b) (units of contour lines: m for coal thickness and m³/t for gas content with different color areas).

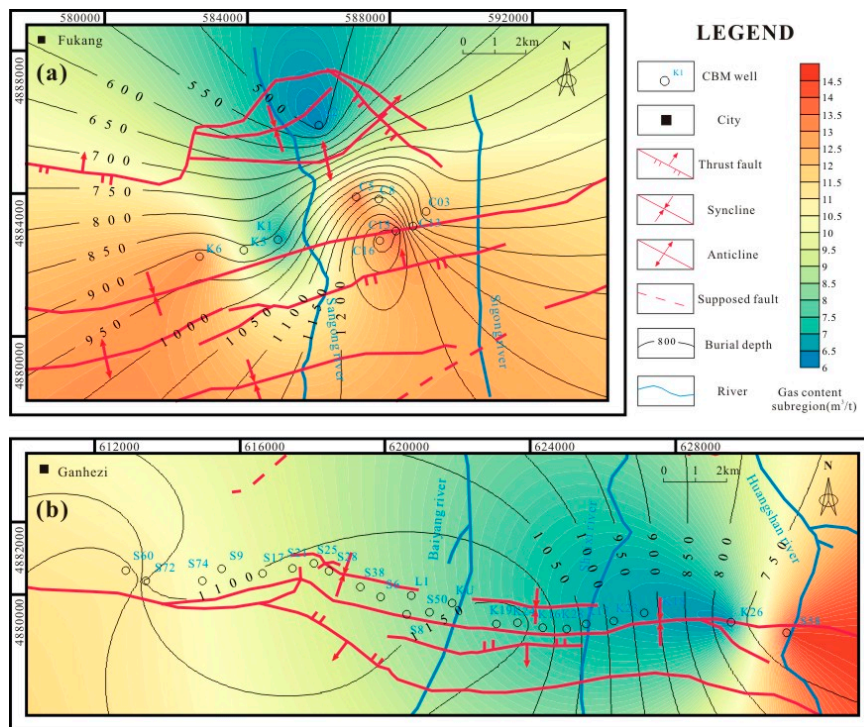


Figure 10. Relationship between gas content and burial depth of No. 43 coal seam in the Fukang syncline (a) and Ergonghe syncline (b) (units of contour lines: m for burial depth and m³/t for gas content with different color areas).

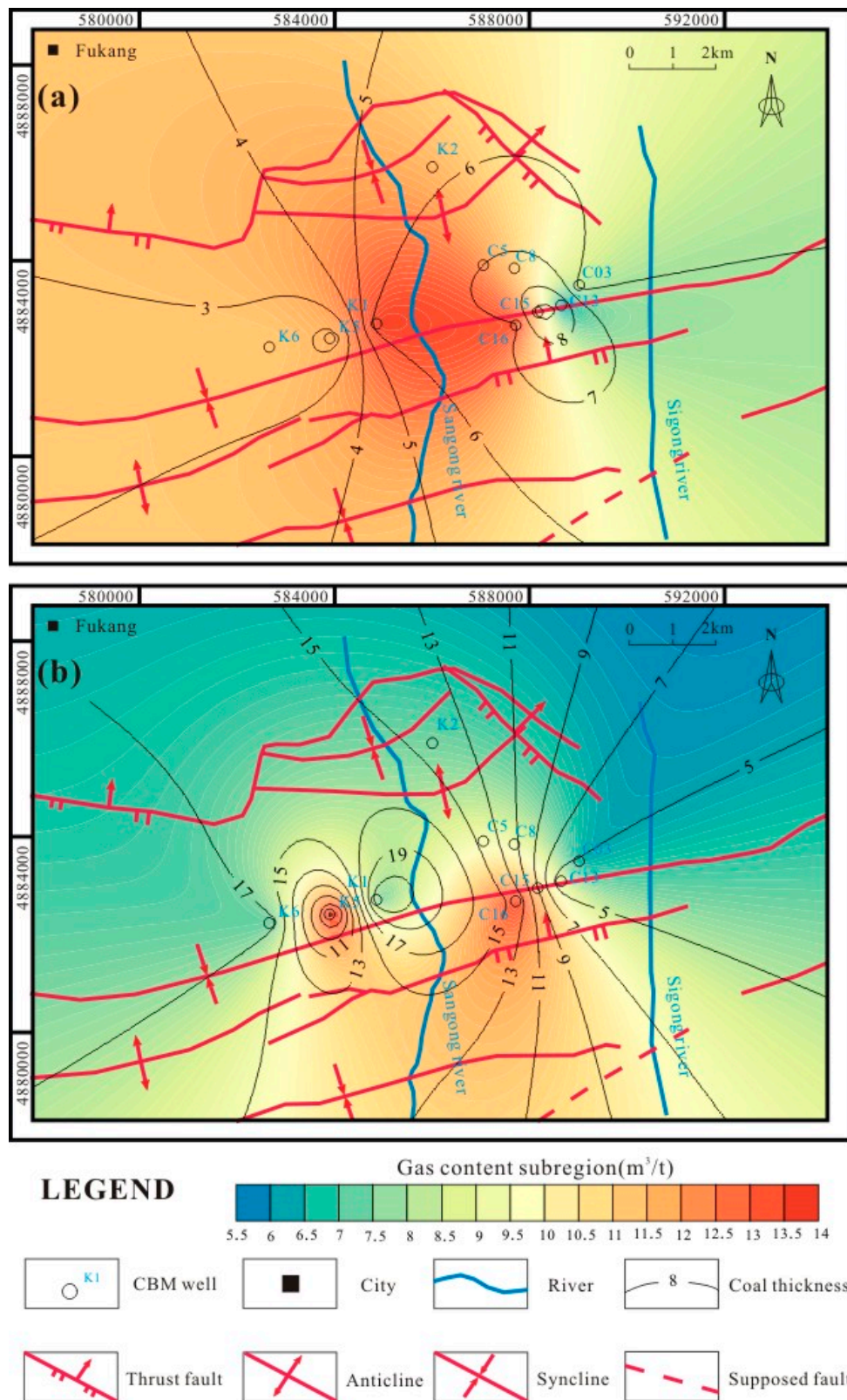


Figure 11. Relationship between gas content and coal thickness of Nos. 45-1 (a) and 45-2 (b) coal seams in the Fukang syncline (units of contour lines: m for coal thickness and m^3/t for gas content with different color areas).

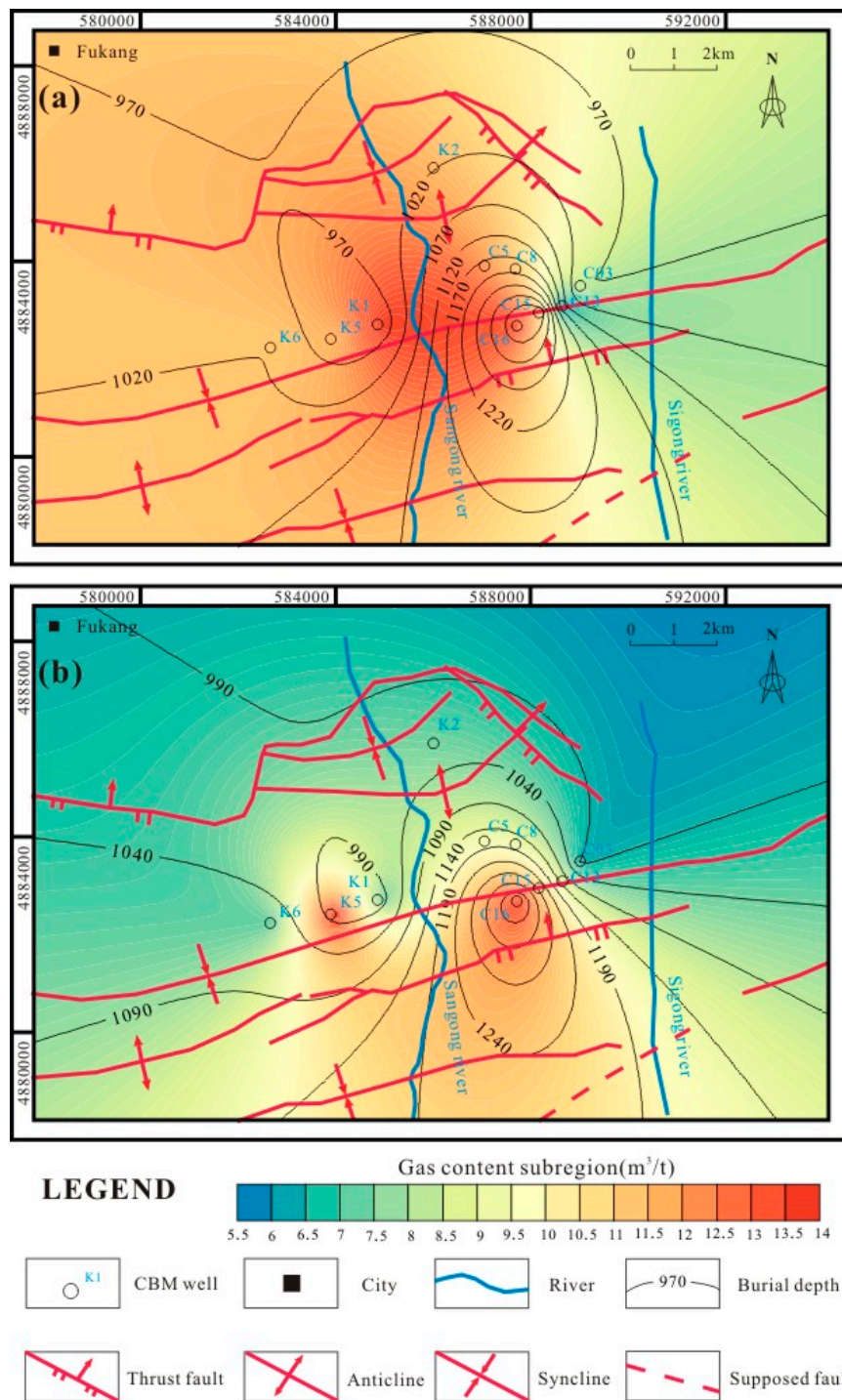


Figure 12. Relationship between gas content and burial depth of No. 45-1 (a) and 45-2 (b) coal seams in the Fukang syncline (units of contour lines: m for burial depth and m^3/t for gas content with different color areas).

4.2. Geological Factors Affecting Gas Content

4.2.1. Geological Structure Controls

In the modern SJB, a few faults and folds with W–E axial striking are common (Figure 1). These structures induce coal deformation. The coal reservoir permeability is relatively low, with maximum

values approaching 4 mD. Particularly in cases where strong deformation caused coal mylonitization, the coal reservoir has extreme low permeability. Previous studies indicated that the folds in the SJB were formed by N–S compressional stress during the Himalaya Orogeny [32].

CBM tends to concentrate in the syncline and dissipate in the anticline and normal fault zone [1,26]. In the study area, anticline is less developed, CBM accumulation is mainly controlled by the Fukang syncline and Ergonghe syncline. In the west zone, most of the CBM exploration wells are deployed along the synclinal axis or synclinal wing; the gas content in the axis is significantly high, ranging from 8.43 m³/t to 16.25 m³/t (Table 5). In these synclines, fractures and micropores favorable for CBM concentration are abundant due to the structural stress. The burial depth at axis of syncline is deep and the permeability is low. CBM hardly moves along the vertical direction, and the conditions are conducive to methane accumulation. Therefore, the syncline areas of the SJB are ideal for CBM exploration and development. In the east zone, the Yaomoshan reverse fault cuts through the south wing of Ergonghe syncline, which results in the syncline presenting a monocline form. Figure 7 shows that the gas content closest to the west side of Yaomoshan reverse fault is higher than the east side in the Nos. 39, 41, 42 coal seams because of the fault coating effect. Based on the well data and prediction, the gas content of the SJB is in the order of syncline (well C15 is 13.6 m³/t) > surrounding reverse fault (well S74 is 12.31 m³/t) > slope of syncline (well K18 is 12.24 m³/t) > slope of anticline (well K2 is 7.8 m³/t) > central of reverse fault (well K19 is 6.52 m³/t), if only geological structure patterns are considered.

Table 5. Gas content of CBM wells in the SJB.

Well	Seam Number	Structural Type	Burial Depth (m)	Gas Content (Average) (m ³ /t)
C84	43	wing	1161–1178	9.37–13 (10.25)
C03	43	axis	888–910	8.46–15.54 (13.56)
C03	45-1	axis	968–986	8.43–14.17 (10.83)
C13	43	axis	1020–1038	11.3–15.88 (13.27)
C13	45-1	axis	1072–1081	9.65
C13	45-2	axis	1122–1125	9.13–10.09 (9.61)
C16	43	axis	1357–1384	10.2–16.25 (14.4)
C16	45-1	axis	1406–1413	15.78–16.18 (16.08)
K1	43	wing	851–869	6.7–10.82 (8.26)
K1	45-2	wing	948–971	6.66–11.21 (7.98)
K2	43	wing	469–486	6.93–9.09 (7.8)
K6	45-2	wing	1050–1070	7.56–8.14 (7.8)

Refer to Figure 9 for CBM well locations.

4.2.2. Coal Thickness and Burial Depth

Although the correlation between gas content and coal thickness is positive, the correlation coefficient is low (Figure 13b). In the west zone, the thickness of the No. 39 coal seam is between 6 m and 20 m (Figure 7a), and the thickness of the No. 41 coal seam is 5–19 m (Figure 7b); high gas content is distributed in the area with thickness from 11 m to 19 m. The gas content in the No. 42 coal seam is not related to the thickness (Figure 7c). Gas diffusion and flow are the main patterns for CBM escaping. Due to the low permeability of the coal seam, thick coal seams may provide a long distance for gas escaping [11,39]. Therefore, the coal thickness could affect the in situ gas content. In the No. 43 coal seam of the west zone, the coal thickness increases from 5 m to 23 m from west to east (Figure 9a). The east zone has a coal thickness of 7–15 m, and the central area has the maximum coal thickness (Figure 9b). The thickness of the No. 45-1 coal gradually increases from west to east (Figure 11a), and that of the No. 45-2 coal seam gradually pinches from west to east (Figure 11b); the gas content seems to have no relationship with coal thickness.

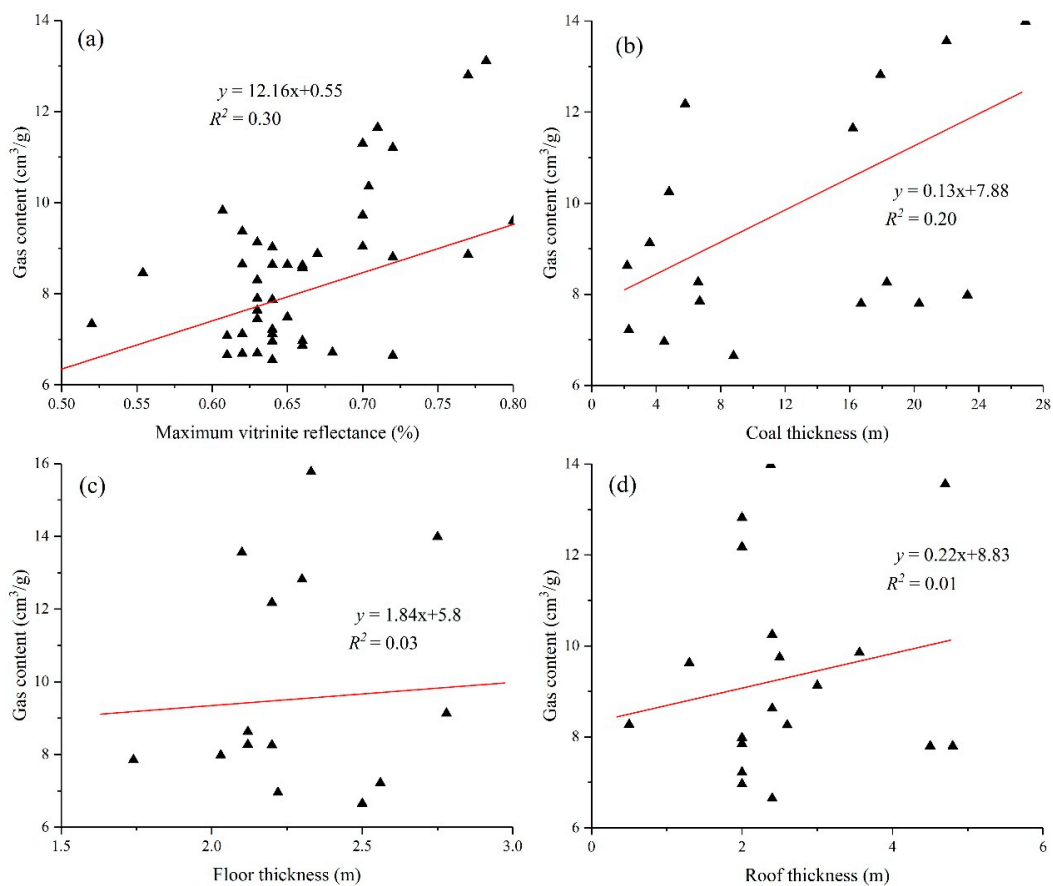


Figure 13. Scatter plots of gas content versus the maximum vitrinite reflectance (a), coal thickness (b), floor thickness (c), and roof thickness (d) in the Fukang syncline and Ergonghe syncline, SJB.

Burial depth is another important gas controlling factor [40]. The burial depth of coals controls the coalification and gas generation [41]. Increasing burial depth can prevent gas dissipation. Moreover, the increasing stress makes the coal permeability decrease, which is conducive to the gas preservation. Figure 14a shows a good correlation between gas content and the burial depth of Nos. 42, 43, and 45 coal seams, $R^2 = 0.56$. However, the relationship between gas content and the burial depth in the Nos. 39 and 41 coal seams is subtle (Figures 8a,b and 14b). When the burial depth reduces from 1000 m to 650 m, the gas content decreases from $13 \text{ m}^3/\text{t}$ to $5.5 \text{ m}^3/\text{t}$ in the No. 42 coal seam from west to east (Figure 8c). In Figure 10a, the burial depth increases from 550 m to 1350 m from north to south, and the gas content increases from $6 \text{ m}^3/\text{t}$ to $13 \text{ m}^3/\text{t}$. The burial depth interval is 750–1200 m from west to east (Figure 10b), and the gas content is $6\text{--}14 \text{ m}^3/\text{t}$. Figure 12 shows that the burial depth of Nos. 45-1 and 45-2 coal seams increases from 970 m to 1440 m, and the gas content increases from $5.5 \text{ m}^3/\text{t}$ to $15 \text{ m}^3/\text{t}$, which indicates that burial depth should be one of the main controlling factors for gas content in the study area.

4.2.3. Coal Metamorphism and Roof Lithology

Deep coal has high metamorphism. Pore structure and gas content are closely dependent on the coal rank [10]. Figure 13a shows that a weak positive correlation between $R_{o,m}$ and gas content ($R^2 = 0.3$) exists, indicating that $R_{o,m}$ may not be the dominant factor for gas content in the study area. Roof lithology is directly controlled by the sedimentary environment, which may include mudstone, limestone, and siltstone [42]. The gas sealing performance of roof lithology is very important for the CBM preservation. The roof lithology with high mud content and thick shale may have a better sealing capacity than that with sandstone and limestone [9]. The roof lithology in the study area

is mainly mudstone and locally siltstone and sandstone (Figure 15). Mudstone has the best sealing capability for CBM. In well C161, the roof lithology of No. 45-1 coal seam is mudstone, and the gas content is 13.99 m³/t. While the roof lithology of Nos. 43, 45-2 coal seams is sandstone and siltstone, the gas content is 8.24 m³/t and 12.13 m³/t, respectively (Figure 16). The gas content in the mudstone roof reservoir is obviously higher than the gas content in the sandstone roof reservoir. The floor, roof thickness, and gas content have a slight correlation, with coefficients of 0.03 and 0.01, respectively (Figure 13c,d). Multiple reservoir parameters including permeability anisotropy, gas sorption time, and water content may have impacts on gas contents in coal seams [43–49]. Due to the limited reservoir data, the impacts of reservoir properties on gas content will not be elaborated here.

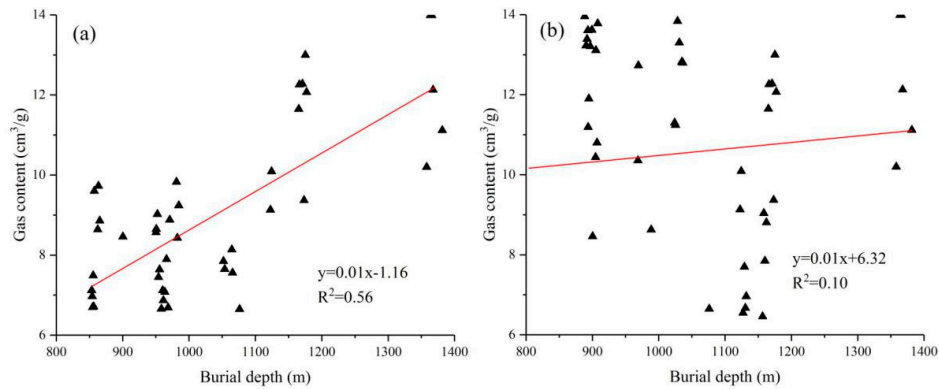


Figure 14. The fitting relationship between the gas content and buried depth of the Nos. 42, 43, 45 coal seams (a); fitting relationship between the gas content and buried depth of the Nos. 39, 41 coal seams (b).

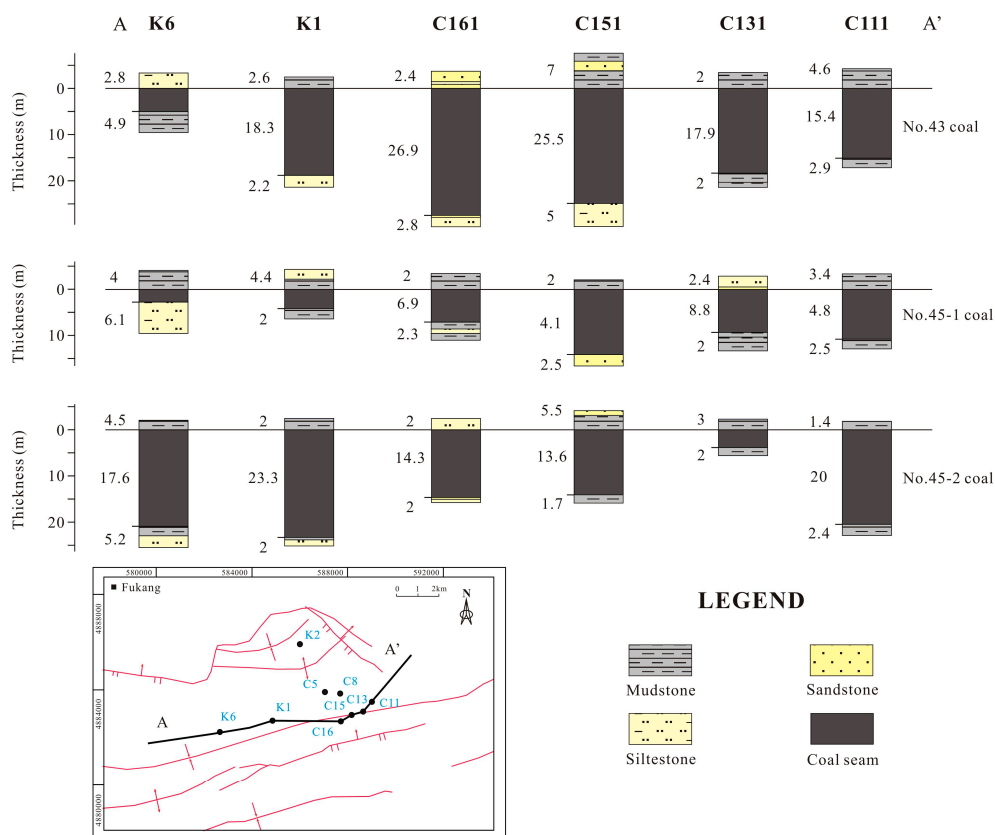


Figure 15. Cross section showing the effects of the roof lithology of the Nos. 43, 45-1, and 45-2 coal seams in the Fukang syncline.

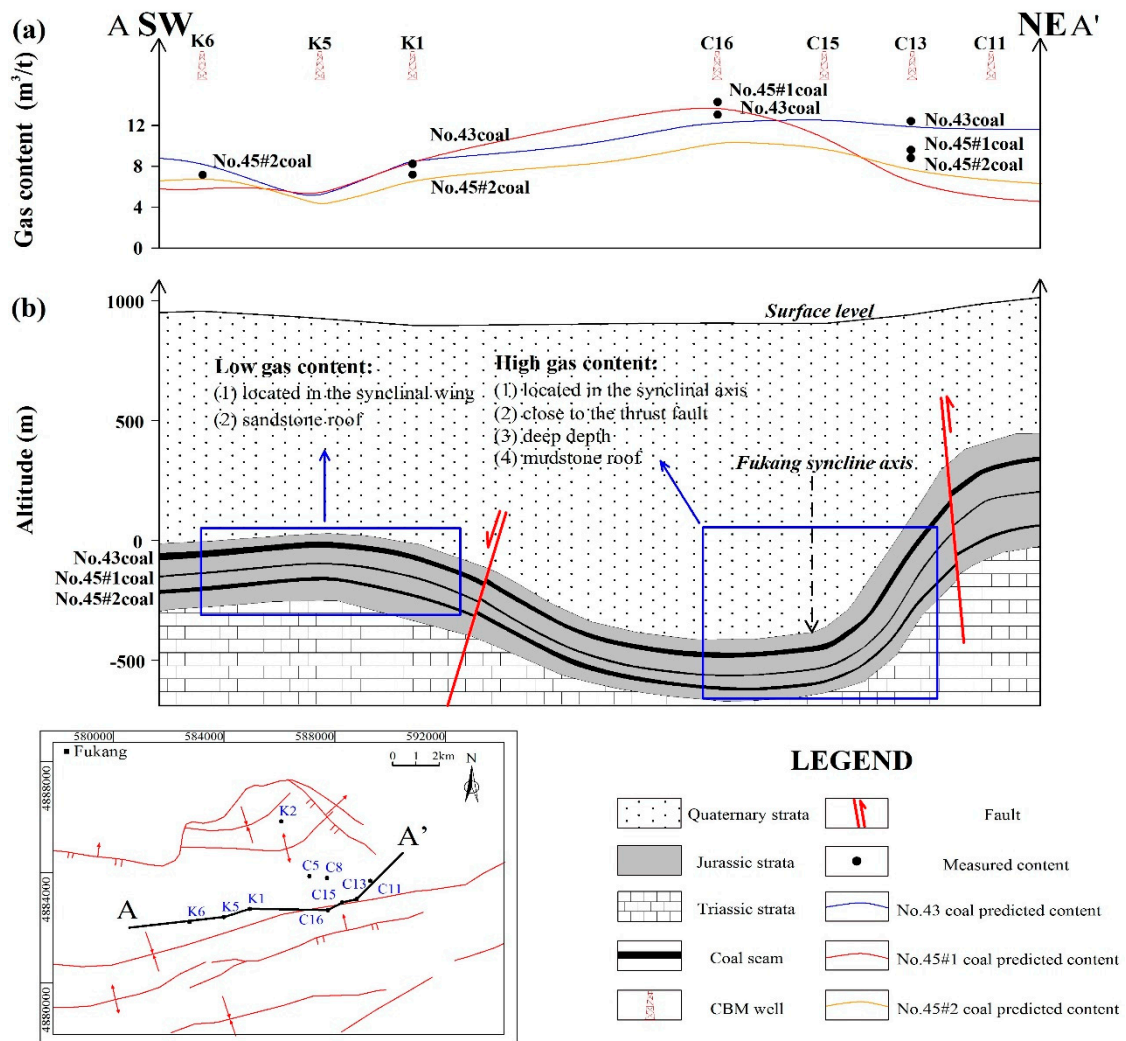


Figure 16. The change of gas content in the SW–NE profile line: (a) the change of gas content in the Nos. 43, 45-1, and 45-2 coal seams; (b) SW–NE structural cross section for low and high gas content.

4.3. Geological Controlling Scenarios of Gas Content

Geological factors affecting the gas content of the Nos. 39, 41, 42, 43, 45-1, and 45-2 coal seams in the study area mainly include geological structure, burial depth, and roof lithology. Figure 16 shows two typical geological scenarios with low gas content and high gas content, which can explain the gas controlling in the SJB. In the SW–NE profile, seven CBM wells with predicted and measured gas content are selected to show the geological controlling scenario of low gas content, as exhibited in Figure 16. The gas content is less than 8 m³/t in the K1, K5, and K6 CBM wells. A normal fault develops in the east of the study area, which results in the gas dissipating easily. This kind of scenario is located in the southern wing of the Fukang syncline. The roof lithology of coal seams here is mostly sandstone, which is unfavorable for gas preservation. Therefore, these factors produce low gas content. The second scenario for high gas content is mainly controlled by the favorable factors including reversed fault, synclinal axis, mudstone roof lithology, and burial depth, where there is a high gas content of 8–13 m³/t as shown in Figure 16. The favorable areas for CBM exploration appear to be a composite gas controlling result of multiple geological factors.

5. Conclusions

Geophysical logging data in the SJB are used to predict the gas content. Methods for predicting gas content including the Kim method, Langmuir method, and well logging method have been compared in detail. Two geophysical logging variables are finally selected to assess the gas content, which has the best fitting relationship with the measured gas content. The predicted results show that the gas content in the study area varies from 4.22 m³/t to 16.26 m³/t. The gas content of the CBM wells along the synclinal axis is significantly higher than that along the synclinal wing in the western zone. In the eastern area, the westward gas content is higher than the eastward gas content in the coal seams because of the fault coating effect by reverse fault. Generally, the gas content of the SJB is in the order of syncline (well C15 is 13.6 m³/t) > surrounding reverse fault (well S74 is 12.31 m³/t) > slope of syncline (well K18 is 12.24 m³/t) > slope of anticline (well K2 is 7.8 m³/t) > central of reverse fault (well K19 is 6.52 m³/t), if only geological structure patterns are considered. Two typical geological scenarios with low gas content and high gas content were revealed. The low gas content is mainly due to the normal fault and the roof lithology of sandstone, whereas the high gas content is mainly controlled by favorable factors including reversed fault, synclinal axis, mudstone roof lithology, and burial depth. The CBM concentration appears to be a composite controlling result of multiple geological factors in the SJB.

Author Contributions: D.L. and Y.C. conceived and designed the experiments; X.G. performed the experiments and wrote the paper; Y.C. and X.G. analyzed the data; D.L., Y.C. and Y.W. revised the paper and provided language support; Y.C. and Y.W. provided technical support.

Funding: This research was funded by the National Major Research Program for Science and Technology of China (Grant no. 2016ZX05043-001) and the National Natural Science Fund of China (Grant nos. 41772160 and 41602170).

Conflicts of Interest: The authors declare no conflict of interest.

References

1. Liu, D.M.; Yao, Y.B.; Tang, D.Z.; Tang, S.H.; Che, Y. Coal reservoir characteristics and coalbed methane resource assessment in Huainan and Huaibei coalfields, Southern North China. *Int. J. Coal Geol.* **2009**, *79*, 97–112. [[CrossRef](#)]
2. Yao, Y.B.; Liu, D.M.; Tang, D.Z. A comprehensive model for evaluating coalbed methane reservoir in China. *J. Geol. Sci. China* **2008**, *82*, 1253–1270.
3. Yao, Y.B.; Liu, D.M.; Tang, D.Z. Preliminary evaluation of the coalbed methane production potential and its geological controls in the Weibei Coalfield, Southeastern Ordos Basin, China. *Int. J. Coal Geol.* **2009**, *78*, 1–15. [[CrossRef](#)]
4. Fu, H.J.; Tang, D.Z.; Xu, T.; Xu, H.; Tao, S.; Li, S.; Yin, Z.Y.; Chen, B.L.; Zhang, C.; Wang, L.L. Characteristics of pore structure and fractal dimension of low-rank coal: A case study of Lower Jurassic Xishanyao coal in the southern Junggar Basin, NW China. *Fuel* **2017**, *193*, 254–264. [[CrossRef](#)]
5. Zhang, J.Y.; Liu, D.M.; Cai, Y.D.; Pan, Z.J.; Yao, Y.B.; Wang, Y.J. Geological and hydrological controls on the accumulation of coalbed methane within the No. 3 coal seam of the southern Qinshui Basin. *Int. J. Coal Geol.* **2017**, *182*, 94–111. [[CrossRef](#)]
6. Karacan, C.Ö.; Ulery, J.P.; Goodman, G.V.R. A numerical evaluation on the effects of impermeable faults on degasification efficiency and methane emissions during underground coal mining. *Int. J. Coal Geol.* **2008**, *75*, 195–203. [[CrossRef](#)]
7. Cai, Y.D.; Liu, D.M.; Yao, Y.B.; Li, J.Q.; Qiu, Y.K. Geological controls on prediction of coalbed methane of No.3 coal seam in Southern Qinshui Basin, North China. *Int. J. Coal Geol.* **2011**, *88*, 101–112. [[CrossRef](#)]
8. Pashin, J.C.; McIntyre-Redden, M.R.; Mann, S.D.; Kopaska-Merkel, D.C.; Varonka, M.; Orem, W. Relationships between water and gas chemistry in mature coalbed methane reservoirs of the Black Warrior Basin. *Int. J. Coal Geol.* **2013**, *126*, 92–105. [[CrossRef](#)]
9. Li, Z.T.; Liu, D.M.; Ranjith, P.G. Geological controls on variable gas concentrations: A case study of the northern Gujiao Block, northwestern Qinshui Basin, China. *Mar. Petrol. Geol.* **2017**, *2*, 1–15. [[CrossRef](#)]

10. Zou, Z.; Liu, D.M.; Cai, Y.D.; Wang, Y.J.; Li, J.P. Geological Factors and Reservoir Properties Affecting the Gas Content of Coal Seams in the Gujiao Area, Northwest Qinshui Basin, China. *Energies* **2018**, *11*, 1044. [[CrossRef](#)]
11. Zhao, J.L.; Tang, D.Z.; Xu, H.; Lu, Y.M.; Tao, S. High production indexes and the key factors in coalbed methane production: A case in the Hancheng block, southeastern Ordos Basin, China. *J. Petrol. Sci. Eng.* **2015**, *130*, 55–67. [[CrossRef](#)]
12. Yu, F.S.; Li, X.J.; Li, D.H.; Feng, Z.C.; Li, X.L. Simulation for the Controlling Factors of Structural Deformation in the Southern Margin of the Junggar Basin. *Acta Geol. Sin-Engl.* **2012**, *86*, 842–853.
13. Estimating Methane Content of Bituminous Coalbeds from Adsorption Data. Available online: <https://www.cdc.gov/niosh/mining/works/coverSheet217.html> (accessed on 11 July 2018).
14. Hawkins, J.M.; Schraufnagel, R.A.; Olszewsk, A.J. Estimating coalbed gas content and sorption isotherm using well log data. In Proceedings of the SPE Annual Technical Conference and Exhibition, Washington, DC, USA, 4–7 October 1992.
15. Karacan, C.Ö. Elastic and shear moduli of coal measure rocks derived from basic well logs using fractal statistics and radial basis functions. *Int. J. Rock Mech. Min. Sci.* **2009**, *46*, 1281–1295. [[CrossRef](#)]
16. Fu, X.H.; Qin, Y. Evaluation of gas content of coalbed methane reservoirs with the aid of geophysical logging technology. *Fuel* **2009**, *88*, 2269–2277. [[CrossRef](#)]
17. Siron, D.L.; Segall, M.P. Influences of depositional environment and diagenesis on geophysical log response in the South Carolina Coastal Plain: Effects of sedimentary fabric and mineralogy. *Sediment Geol.* **1997**, *108*, 163–180. [[CrossRef](#)]
18. Wang, Y.J.; Liu, D.M.; Cai, Y.D.; Yao, Y.B.; Zhou, Y.F. Evaluation of structured coal evolution and distribution by geophysical logging methods in the Gujiao block, northwest qinshui basin, China. *J. Nat. Gas Sci. Eng.* **2018**, *51*, 210–222. [[CrossRef](#)]
19. Mavor, M.J.; Close, J.C.; McBan, R.A. Formation evaluation of exploration coalbed-methane wells. *SPE Form. Eval.* **1994**, *9*, 285–294. [[CrossRef](#)]
20. Hou, J.; Zou, C.C.; Huang, Z.H.; Xiao, L. Comparison of gas content evaluation methods in the log interpretation of coalbed methane. *Adv. Mater. Res.* **2013**, *734*, 1362–1366. [[CrossRef](#)]
21. Bhanja, A.K.; Srivastava, O.P. A new approach to estimate CBM gas content from well logs. In Proceedings of the SPE Asia Pacific Oil and Gas Conference and Exhibition, Perth, Australia, 20–22 October 2008.
22. Liu, Z.D.; Zhao, J.Z. Quantitatively evaluating the CBM reservoir using logging data. *J. Geophys. Eng.* **2016**, *13*, 59–69. [[CrossRef](#)]
23. Peng, C.; Zou, C.C.; Zhou, T.N.; Li, K.; Yang, Y.Q.; Zhang, G.H.; Wang, W.W. Factors affecting coalbed methane (CBM) well productivity in the Shizhuangnan block of southern Qinshui basin, North China: Investigation by geophysical log, experiment and production data. *Fuel* **2017**, *191*, 427–441. [[CrossRef](#)]
24. Sun, P.; Wang, B.; Sun, F.J.; Zhen, G.Q.; Li, G.Z.; Wang, H.Y.; Liu, H.L.; Deng, Z. Research on reservoir patterns of low-rank coal-bed methane in China. *Acta Pet. Sin.* **2009**, *30*, 648–652. (In Chinese)
25. Liu, C.L.; Wang, X.H.; Liu, K.; Wang, J.; Guo, H.; Sun, Z.Q. Occurrence features of coalbed methane in inclined coal seam of Junggar Basin, Xinjiang. *Adv. Mater. Res.* **2014**, *868*, 696–699. [[CrossRef](#)]
26. Fu, H.J.; Tang, D.Z.; Xu, H.; Xu, T.; Chen, B.L.; Hu, P.; Yin, Z.Y.; Wu, P.; He, G.J. Geological characteristics and CBM exploration potential evaluation: A case study in the middle of the southern Junggar Basin, NW China. *J. Nat. Gas. Sci. Eng.* **2016**, *30*, 557–570. [[CrossRef](#)]
27. Guo, J.G.; Pang, X.Q.; Guo, F.T.; Wang, X.L.; Xiang, F.C.; Jiang, F.J.; Wang, P.W.; Xu, J.; Hu, T.; Peng, W.L. Petroleum generation and expulsion characteristics of lower and middle. *Can. J Inform. Lib. Sci.* **2014**, *51*, 537–557.
28. Yuan, Y.; Tang, Y.; Shan, Y.S.; Zhang, J.Q.; Cao, D.Y.; Wang, A.M. Coalbed methane reservoir evaluation in the Manas mining area, southern Junggar Basin. *Energ. Explor. Exploit.* **2018**, *36*, 114–131. [[CrossRef](#)]
29. Fu, H.J.; Tang, D.Z.; Xu, T.; Xu, H.; Tao, S.; Zhao, J.L.; Chen, B.L.; Yin, Z.Y. Preliminary research on CBM enrichment models of low-rank coal and its geological controls: A case study in the middle of the southern Junggar Basin, NW China. *Mar. Petrol. Geol.* **2017**, *83*, 97–110. [[CrossRef](#)]
30. Zheng, G.D.; Ma, X.X.; Guo, Z.F.; Hilton, D.R.; Xu, W.; Liang, S.Y.; Fan, Q.H.; Chen, W.X. Gas geochemistry and methane emission from Dushanzi mud volcanoes in the southern Junggar Basin, NW China. *J. Asian Earth Sci.* **2017**, *149*, 184–190. [[CrossRef](#)]

31. Chen, B.; Arakawa, Y. Elemental and Nd-Sr isotopic geochemistry of granitoids from the west Junggar foldbelt (NW China), with implications for Phanerozoic continental growth. *Geochim. Cosmochim. Acta* **2005**, *5*, 1307–1320. [[CrossRef](#)]
32. Luo, X.R.; Wang, Z.M.; Zhang, L.Q.; Yang, W.; Liu, L.J. Overpressure generation and evolution in a compressional tectonic setting, the southern margin of Junggar Basin, northwestern China. *AAPG Bull.* **2007**, *91*, 1123–1139. [[CrossRef](#)]
33. SAC. *Heating and Desorption Method in Coalbed Methane Content Determination*; GB/T 28753-2012; China National Standardization Management Committee: Beijing, China, 2012.
34. Xiaoyan, L.; Suian, Z.; Xiaozhong, S.; Qiang, W.; Jie, Y. *Method of Determining Coalbed Gas Content*; GB/T 19559-2008; China National Standardization Management Committee: Beijing, China, 2008.
35. Mardon, S.M.; Eble, C.F.; Hower, J.C.; Takacs, K.; Mastalerz, M.; Bustin, R.M. Organic petrology, geochemistry, gas content and gas composition of Middle Pennsylvanian age coal beds in the Eastern Interior (Illinois) Basin: Implications for CBM development and carbon sequestration. *Int. J. Coal Geol.* **2014**, *127*, 56–74. [[CrossRef](#)]
36. Tixier, M.P.; Alger, R.P. Log evaluation of nonmetallic mineral deposits. *Geophysics* **1970**, *35*, 124–142. [[CrossRef](#)]
37. Zhang, Z.Q. On coalbed methane industrial components and gas content calculation model in heshun area. *Well Log. Technol.* **2013**, *37*, 99–102. (In Chinese)
38. Huang, Z.H.; Zou, C.C.; Yang, Y.Q.; Zhang, G.H.; Wang, W.W. Coalbed Methane Reservoir Evaluation from Wireline Logs in TS District, Southern Qinshui Basin. *Geoscience* **2012**, *26*, 1275–1282. (In Chinese)
39. Scott, A.R. Hydrogeologic factors affecting gas content distribution in coal beds. *Int. J. Coal Geol.* **2002**, *50*, 363–387. [[CrossRef](#)]
40. Drobniak, A.; Mastalerz, M.; Rupp, J.; Eaton, N. Evaluation of coalbed gas potential of the Seelyville coal member, Indiana, USA. *Int. J. Coal Geol.* **2004**, *57*, 265–282. [[CrossRef](#)]
41. Ruppert, L.F.; Hower, J.C.; Ryder, R.T.; Levine, J.R.; Trippi, M.H.; Grady, W.C. Geologic controls on thermal maturity patterns in Pennsylvanian coal-bearing rocks in the Appalachian basin. *Int. J. Coal Geol.* **2010**, *81*, 169–181. [[CrossRef](#)]
42. Cai, Y.D.; Liu, D.M.; Zhang, K.M.; Elsworth, D.; Yao, Y.B.; Tang, D.Z. Preliminary evaluation of gas content of the No. 2 coal seam in the Yanchuannan area, southeast Ordos basin, China. *J. Pet. Sci. Eng.* **2014**, *122*, 675–689. [[CrossRef](#)]
43. Salmachi, A.; Bonyadi, M.R.; Sayyafzadeh, M.; Haghghi, M. Identification of potential locations for well placement in developed coalbed methane reservoirs. *Int. J. Coal Geol.* **2014**, *131*, 250–262. [[CrossRef](#)]
44. Salmachi, A.; Karacan, C.Ö. Cross-formational flow of water into coalbed methane reservoirs: Controls on relative permeability curve shape and production profile. *Environ. Earth Sci.* **2017**, *76*, 200–216. [[CrossRef](#)] [[PubMed](#)]
45. Salmachi, A.; Rajabi, M.; Reynolds, P.; Yarmohammadtooski, Z.; Wainman, C. The effect of magmatic intrusions on coalbed methane reservoir characteristics: A case study from the Hoskissons coalbed, Gunnedah Basin, Australia. *Int. J. Coal Geol.* **2016**, *165*, 278–289. [[CrossRef](#)]
46. Salmachi, A.; Dunlop, E.; Rajabi, M.; Yarmohammadtooski, Z.; Begg, S. Investigation of permeability change in ultra-deep coal seams using time-lapse pressure transient analysis: A pilot project in the Cooper Basin, South Australia. *AAPG Bull.* **2018**, *6*, 36–49.
47. Zhu, S.; Salmachi, A.; Du, Z. Two phase rate-transient analysis of a hydraulically fractured coal seam gas well: A case study from the ordos basin, china. *Int. J. Coal Geol.* **2018**, *195*, 47–60. [[CrossRef](#)]
48. Salmachi, A.; Dunlop, E.; Rajabi, M. Drilling data of deep coal seams of the Cooper Basin: Analysis and lessons learned. *J. Aust. Pet. Prod. Explor. Assoc.* **2018**, *58*, 381–394. [[CrossRef](#)]
49. Salmachi, A.; Haghghi, M. Temperature effect on methane sorption and diffusion in coal: Application for thermal recovery from coal seam gas reservoirs. *J. Aust. Pet. Prod. Explor. Assoc.* **2012**, *52*, 291–300. [[CrossRef](#)]

